2013

Anodic Aluminum Oxide (AAO) Membranes for Cellular Devices

Anthony Patrick Ventura
Lehigh University

Anodic Aluminum Oxide (AAO) Membranes for Cellular Devices

by

Anthony P. Ventura

A Thesis

Presented to the Graduate and Research Committee

of Lehigh University

in Candidacy for the Degree of

Master of Science

in

Materials Science and Engineering

Lehigh University

May 2013

This thesis is accepted and approved in partial fulfillment of the requirements for the Master of Science.

_____

Date

_____

Advisor : Wojciech Z. Misiolek

_____

Co-Advisor: Sabrina S. Jedlicka

_____

Chairperson of Department: Helen M. Chan

Acknowledgments

I would like to sincerely thank my advisors, Wojciech Misiolek and Sabrina Jedlicka for their invaluable guidance during the completion of this work. Additionally, I extend my appreciation to the Leowy Family Foundation who has supported my graduate work at Lehigh University. My deepest gratitude goes to Meghan Casey who is responsible for all of the cell culture and immunocytochemistry presented in this thesis. Her hard work and cooperation were essential to the completion of this thesis. I would also like to thank Kylan McQuaig for sharing his AAO knowledge and establishing a fabrication procedure which made this work possible. Bill Mushock assisted a great deal in the SEM analysis of the AAO, and Anne Marie Lobley was a great help in assisting me with my time management. Thanks also go to my colleagues in the Institute for Metal Forming provided positive feedback and critiques of my progress. Finally, I want to thank my family and Beth for always standing by me and pushing me to be a better person in all aspects of my life.

Table of Contents

List of Tables

List of Figures

I. Abstract

Anodic Aluminum Oxide (AAO) membranes can be fabricated with a highly tunable pore structure making them a suitable candidate for cellular hybrid devices with single-molecule selectivity. The objective of this study was to characterize the cellular response of AAO membranes with varying pore sizes to serve as a proof-of-concept for an artificial material/cell synapse system. AAO membranes with pore diameters ranging from 34-117 nm were achieved via anodization at a temperature of -1□C in a 2.7% oxalic acid electrolyte. An operating window was established for this setup to create membranes with through-pore and disordered pore morphologies. C17.2 neural stem cells were seeded onto the membranes and differentiated via serum withdrawal.

The data suggests a highly tunable correlation between AAO pore diameter and differentiated cell populations. Analysis of membranes before and after cell culture indicated no breakdown of the through-pore structure. Immunocytochemistry (ICC) showed that AAO membranes had increased neurite outgrowth when compared to tissue culture treated (TCT) glass, and neurite outgrowth varied with pore diameter. Additionally, lower neuronal percentages were found on AAO as compared to TCT glass; however, neuronal population was also found to vary with pore diameter. Scanning electron microscopy (SEM) and ICC images suggested the presence of a tissue-like layer with a mixed-phenotype population. AAO membranes appear to be an excellent candidate for cellular devices, but more work must be completed to understand the surface chemistry of the AAO membranes as it relates to cellular response.

II. Introduction

II.I Aluminum Anodization

Anodization refers to the electrochemical controlled oxidation of the surface of a metal to increase the thickness of the natural oxide layer. Aluminum anodization in particular, has been effectively utilized in the past century to form protective and aesthetic coatings on aluminum components. Protective coatings consist of a hard Al_2O_3 passivation layer that inhibits environmental interaction with the aluminum component and resists abrasion. Alternatively, under certain conditions anodization produces a porous oxide on the surface of the aluminum allowing for the incorporation of pigments for decorative coatings[1]. Porous coatings, typically referred to as anodic aluminum oxide (AAO), are most typically created using sulfuric acid, oxalic acid or phosphoric acid as an electrolyte[2].

Advances in electron microscopy contributed to increased understanding of porous anodization starting in 1953 when Keller *et al.* observed hexagonally close-packed cells made up of a barrier layer oxide (BLO) and a porous layer. The research concluded that the dimensions of the oxide cells were dependent on the type of electrolyte used as well as the anodizing potential[3]. This study proved to be the basis for future studies by several groups that examined the properties and formation mechanisms of porous oxides on aluminum.

II.II Oxide Growth and Pore Formation Mechanisms

Pores were observed experimentally in AAO but initial pore formation-kinetics studies focused on general oxide growth and ion-diffusion. In 1959, Hoar and Mott

suggested a mechanism for the growth of aluminum oxide from an aluminum substrate. They argued that Al^{3+} ions diffuse through the BLO to neutralize oxide ions formed at the interface between oxide and electrolyte. Simultaneously, OH^- ions diffuse into the oxide to neutralize Al^{3+} ions near the aluminum substrate, resulting in new oxide being formed in the pore bottom and at the Al/oxide interface. The diffusion through the oxide layer is assisted by the electric field[4]. It was later shown that the BLO thickness, which is dependent on the applied voltage during anodization, remained constant during the formation of the porous layer[5].

O'Sullivan and Wood proposed an explanation of the pore formation process and oxide growth with a mechanism that took into account field-assisted dissolution in the bottom of the pores[6]. Figure 1 shows a schematic diagram of the pore growth process. Their work suggested that pore initiation occurs by the merging of locally thickening oxide regions related to the substrate (Al) substructure. Palibroda *et al.* described a discontinuous barrier layer growth process present during anodization wherein electrical breakdown leads to the porous structure[7]. Current density is concentrated on the thinner regions of the BLO, resulting in field-assisted dissolution that is likely thermally enhanced in agreement with the earlier explanation by O'Sullivan and Wood. This theory explained how pores began to form from the BLO during anodization and accounts for the constant thickness of the BLO. The kinetics of this process was described in detail by Patermarakis[8] as well as theoretically modeled by Parkhutik and Shershulsky[9].

Later studies also suggest that there is thermal enhancement resulting in a significant dependence of pore formation on temperature. Pore density was found to decrease with current density and a decrease in temperature due to film growth rate

increases competing with thermal and field-assisted dissolution[10]. As a result of the thermally assisted dissolution in pore bottoms, many anodizations are carried out near 0□ C and some employ ethanol additions to the electrolyte as a coolant[11]. Rigorous stirring is generally required to achieve a desirable pore structure. Belwalkar *et al.* found that pore size and interpore distance were directly related to the applied voltage and inversely related to the electrolyte concentration. Additionally, electrolyte concentration affected growth rate of the AAO pores[12]. Huang *et al.* found that increasing the electrolyte concentration by too much increased dissolutions rates and AAO membranes could no longer be formed[13].

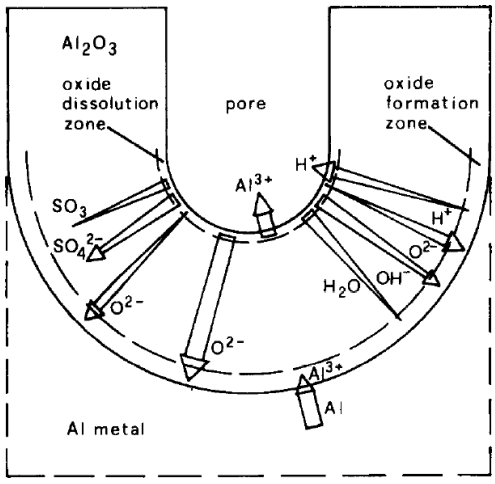

Figure 1. Schematic diagram of the pore formation process depicting ion migration, oxide formation, and oxide dissolution[8]

II.III Self Organization of AAO

Early works on aluminum anodization observed relationships between electrical conditions and cell diameter as well as hexagonally close-packed cells. Pure aluminum is typically used to create self-ordered AAO, as alloying elements typically create defects such as oxygen bubbles in the oxide but it is still possible to form oxygen bubbles and

other defects in pure aluminum[14]. Masuda and Fukuda later investigated the self-ordering as a result of different anodization conditions[15]. It was found that very specific anodization conditions (i.e. electrolyte composition and electrical potential) would produce long-range close-packed pores. Figure 2 demonstrates the increased order observed by Masuda *et al.* as anodization potential increased in sulfuric acid[16]. Figure 3 shows examples of anodization experiments that achieved self-ordered AAO membranes[11,16,17]. These studies showed that using different electrolytes and/or concentrations of electrolytes requires different anodization potentials to achieve self-ordering. This phenomenon was explained by a TEM analysis and numerical study in 2002 by Nielsch *et al.* which they termed the 10% porosity rule[18].

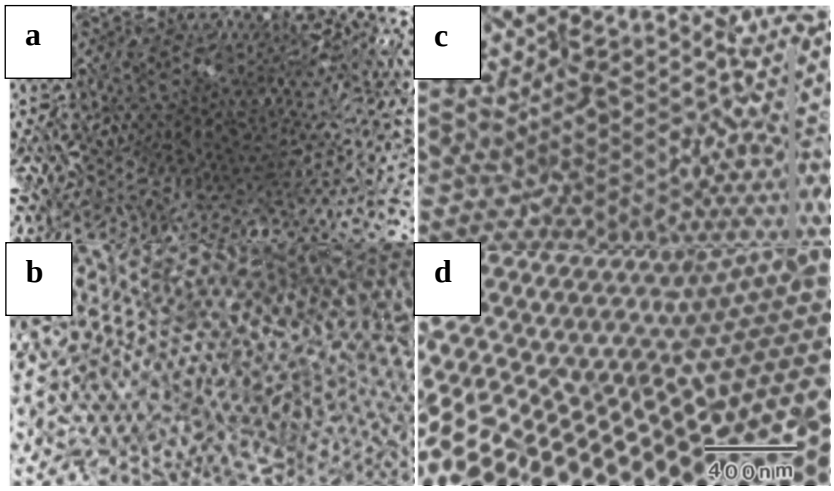

Figure 2. SEM micrographs showing increased order as anodization potential increases in AAO form in 0.3M sulfuric acid at 20(a), 23(b), 25(c), and 27(d) V[16]

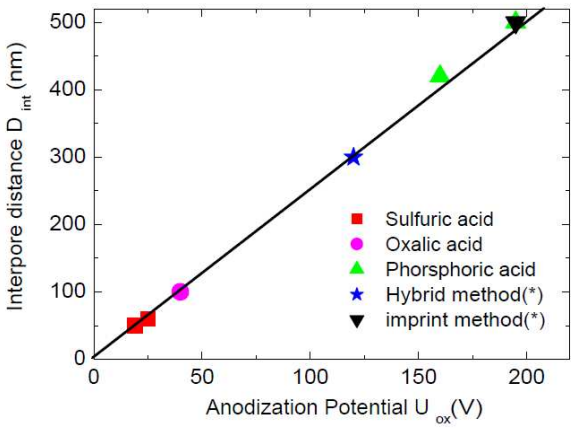

Figure 3. Interpore distance vs. anodization potential conditions that achieve hexagonally close-packed self-organization[11,16,17,19]

Nielsch found that self-ordered AAO could repeatedly be created when the porosity was 10%, independent of the anodization conditions. This number is related to the volume expansion ratio of alumina to aluminum of 1.2. The relationship to the density of aluminum and alumina matches the mechanical stress model of self-organization in which the volume expansion causes repulsive forces between neighboring cells which eventually reach an equilibrium state when they are hexagonally-ordered[11,20]. Therefore, self-ordering is theoretically possible with any interpore distance if cell size and pore diameter are in agreement with the 10% porosity rule as described by Equation 1[18].

$$P = \frac{2\pi}{\sqrt{3}}\left(\frac{r}{D_{int}}\right)^2 \qquad (1)$$

In Equation 1, P is the porosity, r is the pore radius, and D_{int} is the interpore spacing. This equation combined with earlier results which link the anodization potential to the interpore distance and the pH of the electrolyte to the pore radius can be used to create self-ordered AAO over a wide variety of pore sizes as shown in Figure 4[21].

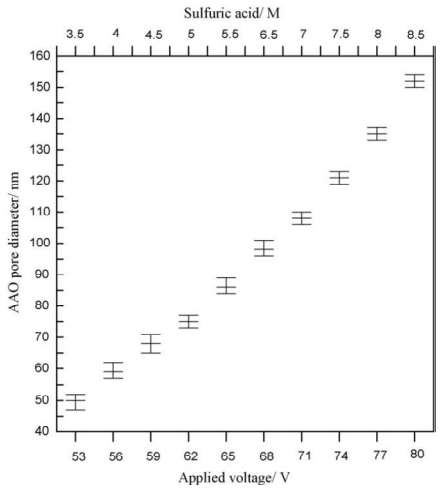

Figure 4. Pore diameter vs. anodization potential and molarity of the sulfuric acid electrolyte which follows the 10% porosity rule to maintain a self-ordered structure[21]

Adding to the 10% porosity rule, Lee *et al.* found that other conditions existed for forming self-ordered AAO at around 3% porosity. The group developed a hard anodization procedure (as opposed to the typical "mild" anodization) that created ordered pores with large interpore distances. Hard anodization is typically used by industry to create low porosity passivation coatings with a high growth rate. The group was able to achieve similar pore sizes as mild anodization in oxalic acid with growth rates an order of magnitude higher. Interpore distance was highly tunable with anodization potential; however, pore size and electrolyte concentration in this new process was not extensively investigated[22].

II.IV Composition and Structure of AAO

Pore formation requires diffusion, which is field assisted, to create new oxide. This new oxide causes a volume expansion which promotes self-ordering. Patermarakis *et al.* described the incorporation of electrolyte ions and H_2O into the AAO regardless of the electrolyte used during anodization. This is schematically depicted in Figure 1[8]. Le

Coz *et al.* categorized three distinct regions in AAO membranes based on TEM studies. The three regions include the pore walls which have ion incorporation, a “pure” aluminum oxide skeleton and so-called interstitial rods at the skeleton triple-points. Figure 5 shows TEM image of the three regions and corresponding x-ray maps showing the incorporation of phosphor from the electrolyte[23]. The x-ray maps follow predictions by earlier work that the skeleton region is denser than the pore walls. The density increase serves to resist migration of ions into neighboring cells[24]

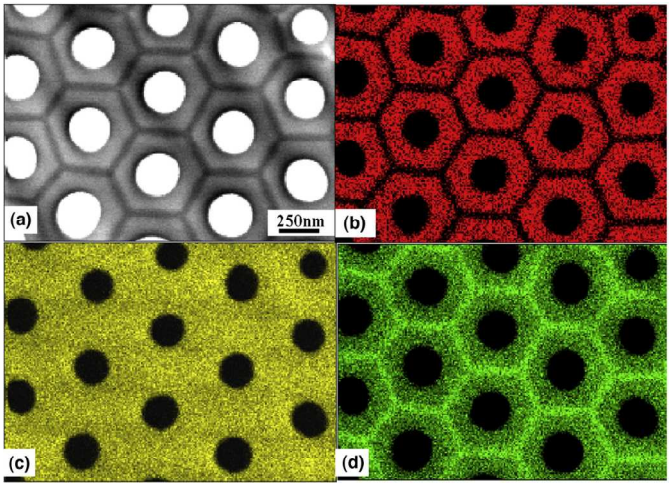

Figure 5. TEM image (a) and corresponding x-ray maps for phosphorous (b), oxygen (c) and aluminum (d) of an AAO membrane anodized in phosphoric acid[23]

TEM studies conducted by Sui *et al.* found that AAO membranes were amorphous throughout[25]. However, Le Coz *et al.* demonstrated that exposure to an electron beam resulted in crystallization of the skeleton region[23]. Other studies were conducted in an attempt to crystallize the entire AAO membrane through thermal treatments. Mardilovich *et al.* studied thermal treatment of AAO membranes up to 1200□C. Crystallization was obtained by heating above 800□C, and the resulting crystal

structure of the alumina depended upon the time and temperature of the thermal treatment. Additionally, heating above 840□C removed impurities as a result of the crystallization process[24]. The same group completed a study on the chemical stability of the amorphous AAO as compared to the crystallized samples. Crystallized AAO displayed exceptionally high resistance to acids and bases. Conversely, amorphous AAO had a narrow range of pH in which it did not partially or fully dissolve regardless of annealing time/temperature below the crystallization conditions[26]. In addition to chemical resistance, McQuaig used nanoindentation to show that there was an increase in membrane hardness by a factor of two as a result of crystallization[27]. Pore integrity was maintained throughout the heat treatments in both studies.

II.V Current Two-Step AAO Fabrication

The studies mentioned thus far have provided a solid basis for some common AAO fabrication principles to be established. The effect of electrical potential and electrolyte choice/composition on the porous cell geometry and self-organization is fairly well understood[3,6,8,18,21]. Many current fabrication processes utilize the two-step anodization originally proposed by Masuda and Fukuda to create pore initiation sites during the first anodization[17]. The chemical removal of the oxide layer grown during the first step leaves behind a patterned aluminum surface that leads to stable pore growth during subsequent anodizations[28]. Sulka *et al.* also found that there was no significant benefit to more etch-anodization cycles in terms of pore organization[29]. If an organized pore structure is desired, nano-patterning via lithography or stamping can be used to tailor pore geometry and ordering successfully[17].

II.VI Biological Applications of AAO

AAO membranes have seen extensive research as templates for various nanostructures, data storage devices, energy generation and storage, and drug delivery[2,30–32]. Polycrystalline alumina as well as AAO is chemically stable and biocompatible. AAO also exhibits very low autofluorescence making it suitable for many biological imaging techniques[33]. Furthermore, AAO fabrication is industrially-scalable, which is not the case for many other techniques such as lithography[11,34]. AAO also lends itself well to many surface modification approaches, including molecular self-assembly, layer-by-layer deposition, plasma polymerization, atomic layer deposition, dip coating, chemical vapor deposition and electrochemical metal deposition[35–38]. These properties, in combination with the uniquely tunable pore structure with high aspect ratio, give AAO unique capabilities in many biological and chemical sensing applications.

While the autofluorescence of AAO is generally low, the photoluminescence of AAO depends on many fabrication parameters. The potential, pore diameter, thermal treatment and anodization regime all affect the photoluminescent properties[35,36,39]. Surface-plasmon resonance (SPR) and variations of the technique are widely used to study biological interactions, namely protein adsorption behavior. Plasmonic properties of surfaces rely strongly on the refractive index of the adjacent medium (in this case an AAO membrane). This allows for hybrid metal-AAO devices that have successfully been used to study the adsorption and desorption of bovine serum albumin (BSA) under different pH and bioaffinity conditions[40,41]. AAO has also been investigated to replace the use of silicon in reflectometric interference spectroscopy (RIfS) due to its improved chemical stability and more defined pore structure[42]. RIfS is based on the interaction of

white light with thin films to study the surface conditions and adsorption of any molecules of interest to act as a sensor[43]. Most notably, AAO substrates have been utilized for label-free detection of complementary DNA with improved sensitivity[44].

AAO is an electrical insulator, so current tends to flow entirely through the pore channels when AAO is used as a component in an electrical system. Impedance spectroscopy (IS) measures the dielectric properties of a material by making use of this effect. The pores can contain biological events while simultaneously monitoring changes in conductivity/impedance[45,46]. Furthermore, with some surface modification, AAO's electrical properties can be modified to create devices that can measure changes in electrochemical response. The result is ultra-sensitive nanobiosensors for the detection of viruses using specific antibodies immobilized inside of the pores. In some cases, this effect can be enhanced using gold nanoparticles to block the pore openings[47–50].

An area of particular interest is use of the membranes for high-throughput microbiology and cellular hybrid devices. The high surface-to-volume ratio of AAO and tunable pore morphology results in a biocompatible substrate that has single molecule sensitivity[31]. Karlsson *et al.* studied the in vitro interaction of human osteoblast-like cells (HOBs) with AAO for use in orthopedic inserts[51]. The study found that HOBs spread and adhered well to the AAO surface and the osteoblastic phenotype was retained on the alumina. Additionally, although some Al^{3+} ions were measured in the surrounding culture media, the result was insignificant and did not have any adverse effects on the HOB development. However, this study was limited to AAO with 200nm pores and only studied the response of the HOBs, no other cell types. Hu *et al.* investigated cell culture on AAO substrates and introduced geometric constraints as well as a varying pore size[52].

NIH 3T3 cells were seeded onto AAO substrates with pore sizes varying from 75-300nm. Geometrical constraints in the form of a polydimethylsiloxane (PDMS) film allowed for selected adhesion of the cells. The group also found that cell adhesion on the AAO substrates of small pore sizes was much faster than on flat surfaces but not for larger pore sizes as shown in Figure 6. However, to achieve the pore size range in this study the electrolyte composition was varied and oxalic and phosphoric acid electrolytes were used. The control for this experiment was a smooth aluminum surface, and while this lacks the topography of the AAO, it is also different chemically which is not accounted for when comparing the cell adhesion.

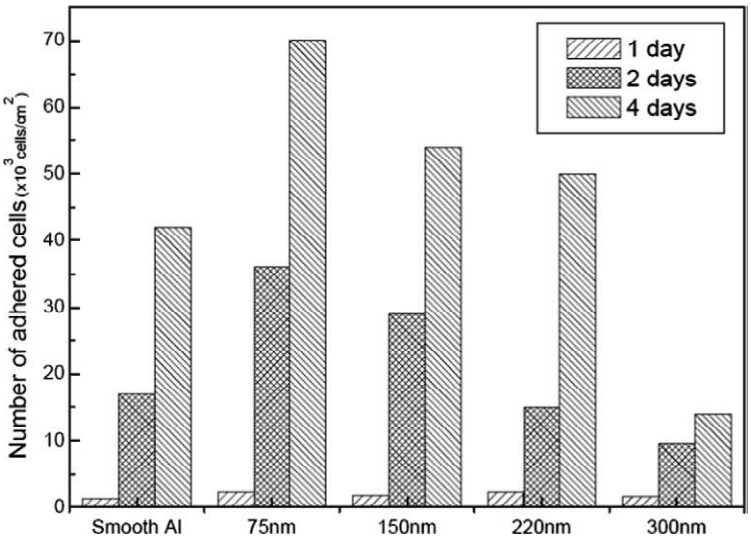

Figure 6. Number of cells adhered on a smoothly polished aluminum foil and AAO substrates with varying pore size after 1, 2 and 4 days[52]

III. Research Objective

The objective of this research is to characterize the cellular response of C17.2 neural stem cells (NSCs) on AAO substrates with varying pore sizes. Chemical

differences between the AAO substrates will be minimized by utilizing the same electrolyte composition and procedure for the fabrication of all membranes. This work will use neuronal differentiation of the NSCs as a proof-of-concept study for the use of AAO in an artificial cell/material synapse system.

IV. Experimental Procedure

IV.I AAO Fabrication

Previous work by McQuaig and Belwalker *et al.* was used as a basis for a flexible anodization procedure to create AAO with pore sizes ranging from ~30-120nm[12,27]. 99.99% pure aluminum foil with a thickness of 0.1 mm in the as-rolled condition was used as a starting substrate for anodization. Pure aluminum was used to reduce the number of defects present in the AAO and promote a robust pore structure. Although annealed aluminum promotes long-range ordering by limiting the number grain boundaries in the substrate, long range highly ordered pores were not the primary goal of this experiment so the foil was used in the as-rolled condition[2]. Aluminum foil that was thicker than 0.1 mm could not be used with this procedure to create AAO membrane due to the nature of the chemical removal of the aluminum substrate. The foil was cut into approximately 3.0 cm by 5.0 cm rectangles and ultrasonically degreased in acetone for 5 minutes. The aluminum was then electropolished to remove processing lines and create a smooth surface for anodization. Electropolishing was carried out at 6.5 Amps in a mixture of phosphoric acid, ethanol, and deionized water prior to anodization.

Initial work used ice packed around a beaker in an insulated enclosure to maintain a constant temperature in the anodization chamber. This method proved to be unreliable

and create varying electrical conditions due to gradually increasing temperature throughout the fabrication process and was ultimately replaced. Figure 7 shows a picture of the finalized anodization chamber setup used in this experiment. A recirculating chiller connected to a double-walled beaker was used to keep the anodization chamber at a constant temperature of -1 □C. A 1:1 ratio of ethylene glycol and deionized water was used as the cooling fluid. Threaded copper rods were attached to a polycarbonate lid and soldered to alligator clips which held the aluminum foil and cathode. Graphite foil with a thickness of 0.13 mm and the same dimensions as the aluminum foil was used as a cathode for this experiment. The threaded copper rods were connected to a rack power supply to vary the voltage during anodization.

Figure 7. Recirculating chiller and double-walled beaker used as the anodization chamber in this experiment

A 2.7 wt% oxalic acid, 10 wt% ethanol, and 87.3 wt% deionized water solution was used for all anodization steps. Oxalic acid was chosen as an electrolyte because it has been shown to favor the growth of pores with a constant diameter through the entire

thickness of the membrane[53]. The small addition of ethanol to the oxalic acid mixture acts as a coolant and prevents the mixture from freezing at a temperature of -1 □C. The solution was replaced between each membrane fabrication, but not in between anodization steps for a single membrane. A pre-anodization is carried out at a temperature of -1 □C for 5 minutes in the oxalic acid solution. This step was required after electropolishing to promote the adherence of a polymer film that restricts membrane growth to only one side of the aluminum foil. Membrane growth was restricted for easier removal of the AAO from the aluminum substrate.

The first anodization step was run for 2 hours to create pore initiation sites. The voltage during this step was varied from 25V-55V in order to change the final pore size of the AAO membrane. It is likely that this voltage range could be altered or expanded by changing the composition of the electrolyte but this was avoided in order to limit chemical changes during membrane fabrication. After the first anodization, the oxide layer was etched away in a mixture of 2 wt % chromic acid, 4 wt% phosphoric acid and 94 wt% deionized water at a temperature of 65 □C. After this etching step, the entire oxide layer is removed and the patterned aluminum surface is left for the second anodization step.

The second anodization step was carried out at 40V for around 40 hours in the same oxalic acid solution at a temperature of -1 □C. Anodization at 40V provided an adequate oxide-growth rate without generating excess heat. The long anodization time results in a membrane that is thick enough to adequately handle the stresses encountered during cell culture and analysis. Acetone was used to remove the polymer film after the anodization is complete. The aluminum substrate was then removed chemically by

etching in a mixture of 4 wt% copper chloride, 10 wt% hydrochloric acid, and 86 wt% deionized water at room temperature. The time to etch away the aluminum can vary slightly, and care must be taken to only etch as long as necessary to limit the chemical attack on the AAO membrane. The final etching step was completed at a temperature of 35 □C in a 0.1M solution of phosphoric acid for 80 minutes with periodic agitation. This step removes the BLO and leaves only the completed AAO membrane with through-pores. Although leaving the BLO intact would improve the mechanical stability of the membranes, it was removed in later AAO fabrication to ease the simplify sample tracking during cell culture. The entire membrane fabrication procedure and solutions used for each step are shown in Table 1and Table 2, respectively.

Table 1. Anodization procedure used in this experiment to fabricate AAO membranes with pore sizes ranging from 30-80nm

Step	**Solution**	**Time**	**Temperature**	**Electrical Conditions**
Electropolishing	A	40 s	22 □C	6.5 Amps
Pre-Anodization	B	5 min	-1 □C	20 V
1st Anodization	B	2 hr	-1 □C	Varied
1st Etch	C	1 hr	65 □C	---
2nd Anodization	B	40 hr	-1 □C	40V
2nd Etch	D	6 hr	22 □C	---
3rd Etch	E	80 min	30 □C	---

Table 2. List of solutions and corresponding compositions used during the AAO fabrication process

Solution	Composition
A	45 vol% Phosphoric Acid, 36 vol% Ethanol, Balance DI H_2O
B	2.7 wt% Oxalic Acid, 10 wt% Ethanol, Balance DI H_2O
C	2 wt% Chromic Acid, 4 wt% Phosphoric Acid, Balance DI H_2O
D	4 wt% $CuCl_2$, 10 wt% Hydrochloric Acid, Balance DI H_2O
E	0.1M Phosphoric Acid

IV.II AAO SEM Analysis and Pore Characterization

Portions of each AAO membrane were set aside prior to cell growth for scanning electron microscopy analysis to characterize the pore size and structure. Each sample was coated with iridium for 15 seconds to create a conductive surface layer. The top and bottom of each membrane was imaged to compare the pore structures across the membrane thickness. Pore size was measured from the SEM images using ImageJ software. Assuming circular pores, the pore diameter was taken as the average of a minimum of 100 pores from three separate fields of view on only one side of the membrane.

IV.III Polycrystalline Alumina Controls

Polycrystalline Al_2O_3 was chosen as a control for cellular response studies. The alumina control samples have similar chemistry to the AAO but lack the porous and topographic features which are the subject of investigation in this study. AKP-HP Al_2O_3

powder from the Sumitomo Company with a mean particle size of 0.45 µm was spark plasma sintered to form the polycrystalline alumina samples. The powder was placed in a graphite die and held at 10 MPa and 700 □C for 30 minutes to burn off any organic impurities. Following a ramp up to 1300 □C and 60MPa, the samples were held for 25minutes to sinter the particles and create alumina cylinders that were approximately 20mm diameter by 8mm long. The alumina was then sectioned using a high-speed diamond blade into thin sheets for cell culture.

IV.IV Sterilization and Preparation for Cell Culture

In preparation for cell culture, the AAO membranes and polycrystalline alumina were first UV sterilized overnight. The membranes were then washed with sterile 1X Phosphate Buffered Saline (PBS), followed by a 30 minute wash with growth medium (GM) [high glucose Dulbecco's Modified Eagle Medium (DMEM), supplemented with 10% Fetal Bovine Serum (FBS), 5% Horse Serum (HS), 1% L-glutamine]. The membranes were incubated in GM overnight at 37°C and 5% CO_2[54].

IV.V C17.2 Neural Stem Cell Culture

The C17.2 NSCs that were chosen for this study are an engineered multipotent neural progenitor cell line. They were developed by Snyder *et al.* and are isolated from mouse cerebellum. The cells have also been introduced to living mice brains and were shown to integrate well[55–57]. Most importantly, however, is that C17.2s are similar to human neural stem cells and therefore offer a good model to understand cell response before moving to human cells.

C17.2 NSCs were routinely maintained in GM. The NSCs were seeded onto the AAO membranes at 10,000 cells/cm^2 and incubated at 37°C and 5% CO_2. The cells grew

on the membranes for 2 days before starting a serum-withdrawal protocol promote differentiation of the NSCs. Half of the total volume of media was removed and replaced with serum-free (DMEM high glucose with 1% L-glutamine) media every 2 days. The cells grew on the membranes for 14 days after the serum concentration had dropped below 1%[54].

IV.VI Immunocytochemistry and SEM Analysis of Cell Growth

The primary analysis of cell growth consisted of immunocytochemistry (ICC), qualitative measurements of neurite growth and concentration, and qualitative SEM image analysis of cellular focal adhesion to the membrane surface. Following the serum withdrawal, the cells were formalin fixed and analyzed for neuronal and astrocytic differentiation using β-tubulin III (1:1000, Covance #A488-435L, neuronal) and glial fibrillary acidic protein (GFAP) (1:500, Sigma #C9205, astrocytic) antibodies, respectively. Additional samples were analyzed with nestin (1:100, Developmental Studies Hybridoma Bank #Rat-401, NSCs) and neurofilament H/M (1:100, Covance #SMI-33R, neuronal) antibodies. Nuclei were counter-stained with Hoechst 33258 dye. The β-tubulin III stained samples were used for neurite measurements in NeuronJ to determine the neurite outgrowth length and the neuronal population percentage[54]. For SEM analysis, the cells were fixed in 5% glutaraldehyde followed by dehydration via ethanol and hexamethyldisilazane incubations. The samples were then coated with iridium and observed at low voltage (3keV) to minimize charging and damage to the cells.

V. Results and Discussion

V.I Anodization Optimization

Figure 8 shows an SEM image of the bottom layer of an AAO membrane before the BLO was removed in the final etching step. The image shows successful pore initiation sites with hexagonal ordering as predicted by literature. The top right of the image shows deviation from the hexagonal close packing due to a boundary with another domain of hexagonally ordered cells. Initially, the BLO was not going to be removed in order to make the AAO membranes more robust for handling. However, AAO membranes are optically translucent and difficult to keep in the same orientation throughout cell culture and analysis. In order to ensure cell growth occurred on a porous surface in line with the research objective of this study, the BLO was removed resulting in both surfaces of the AAO to be porous. Cell culture and subsequent biological analysis requires significant handling and the fragility of AAO was seen as a potential issue. Great care was taken with the AAO during these procedures and the mechanical stability of through-pore AAO was found to be sufficient for lab-based studies.

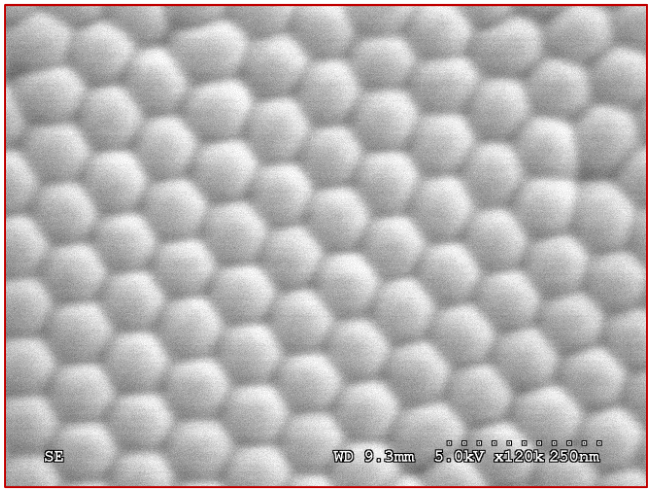

Figure 8. SEM image of the BLO of an AAO membrane used in this study

Literature has shown that rigorous stirring is required during anodization to distribute heat, replenish fresh electrolyte in the growth region, and remove hydrogen bubbles from the surface of the cathode. Traditional mechanical stirring was difficult to implement in the setup used for anodization in this experiment, so air-stirring with compressed air and a diffusing stone was used. Figure 9 shows the bottom and top surfaces of a membrane that was fabricated using rigorous air-stirring. Although the pores initially started out circular with some short-range order, after the full second anodization there was significant pore structure degradation referred to as “pig-nosing” (PN) as seem in the right image of Figure 9. Pig-nosing is characterized by a “pore-in-pore” structure which does not have the straight-channel pores desired for molecular filtering applications. This structure typically results from excess heat generated in the pore-bottoms, or more generally because of instability in the oxide-growth in the pore bottoms. Initial growths proved that air-stirring was ineffective at preventing pig-nosed structures in this setup. However, pig-nosed membranes were used in cell studies as a means of investigating the effect of a degraded pore structure on cell growth. As an estimation, the pore size for pig-nosed membranes was taken to be the distance between the alumina “skeleton” at the center of the cell walls.

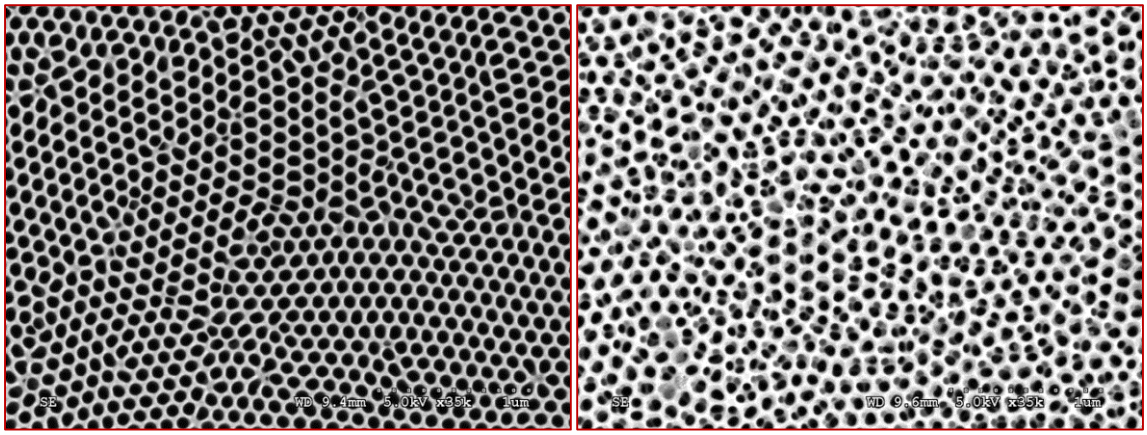

Figure 9. AAO membrane bottom (left) and top (right) surfaces after a first anodization of 40V and a second anodization of 40V for 42 hours with air stirring

Figure 10 shows a membrane fabricated under the same conditions as Figure 9 but without any stirring during anodization. The bottom of the pore openings appear similar, however the top surface of the membrane is slightly different. Although the top surface does not contain ordered-pore domains, each pore is self-contained. There is no “pore-in-pore” morphology that is characteristic of the pig-nosed structure. Additionally, the nominal pore sizes on both surfaces in Figure 10 are within the standard deviation of each other, which is not the case for the membrane in Figure 9. As a result, membranes with this variance in structure were deemed acceptable for cell culture, bearing in mind that pore size and proof of concept for cellular devices is the principle purpose of this investigation. Therefore, all the membranes used for cellular characterization were made without any stirring in the anodization chamber.

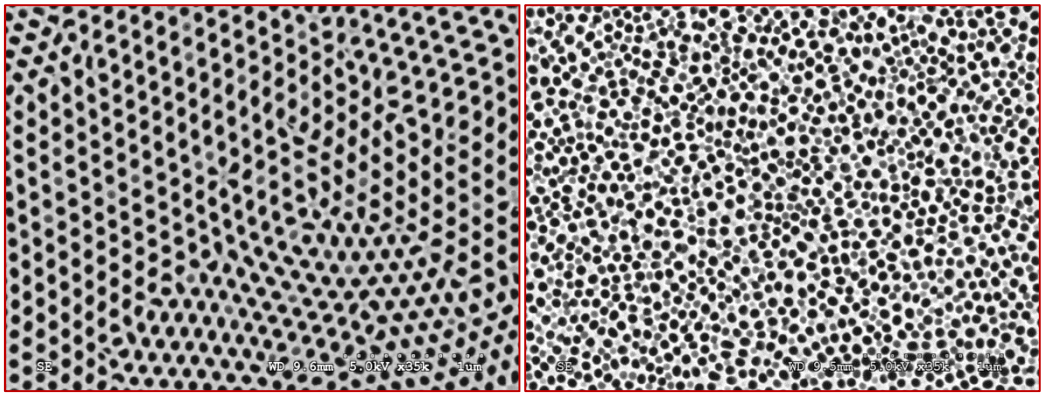

Figure 10. AAO membrane bottom (left) and top (right) surfaces after a first anodization of 40V and a second anodization of 40V for 42 hours without any stirring

Figure 11 shows the first anodization conditions vs. the pore size for the membranes grown for cellular response studies. For the electrolyte and setup used in this experiment, 25V appears to be the threshold for creating satisfactory pore initiation sites. Lower voltages had growth rates that were too low to create a significant oxide layer after 2 hours, resulting in highly disordered and degraded pore structures in the final AAO membranes. Additionally, above around 55V significant heat was generated that cannot be transported away from the growth surface quickly enough. The result was significantly inter-grown pores that cannot be traditionally characterized with pore size and compared to the membranes used in this experiment. Above 45V pig-nosed membranes typically form due to the increased heat generated during anodization. Around 45V (corresponding to about 80nm pores), it is difficult to predict whether a pig-nose structure will develop. As a result, membranes with very similar pore sizes were fabricated in this regime with the two distinct structures observed in this experiment. Note that error bars are present for all measurements of the pore diameter, but the values are minimal for membranes that did

not show the pig-nosed structure. Figure 12 shows SEM images of each of the membranes grown in this experiment.

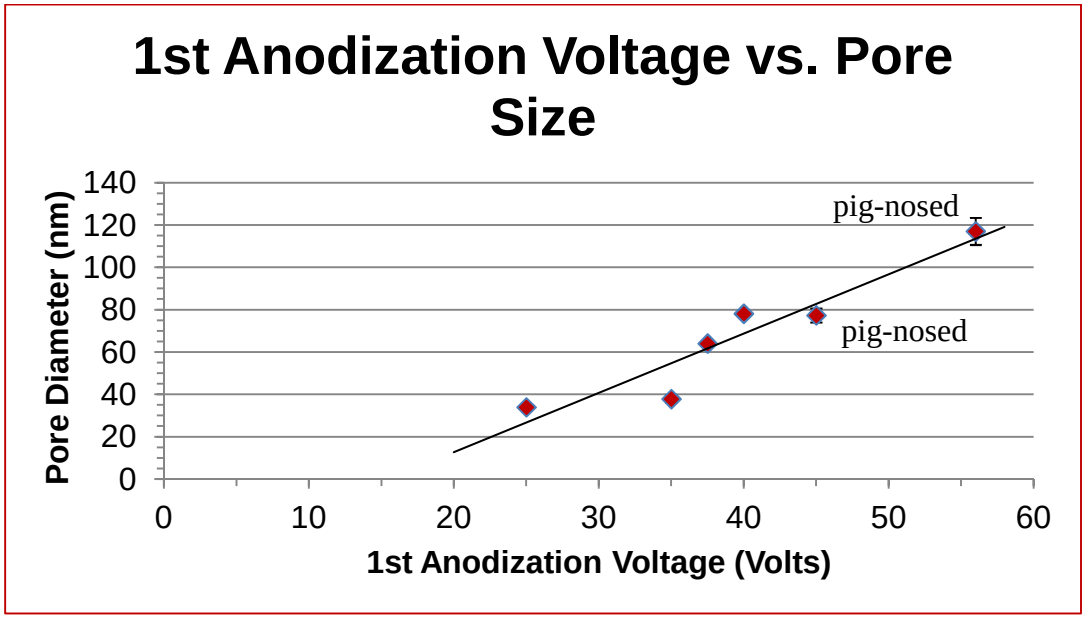

Figure 11. 1st anodization voltage vs. pore size measured for the AAO membranes grown in this study

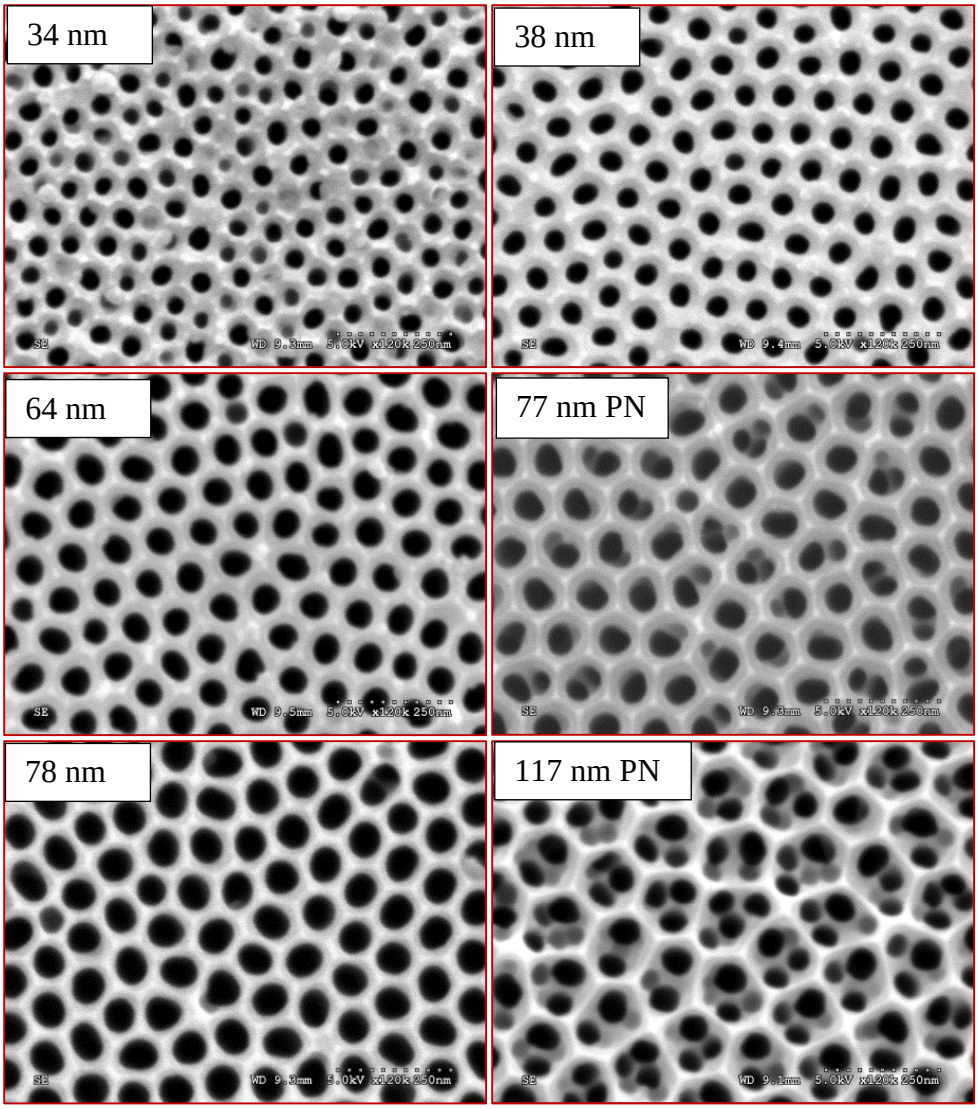

Figure 12. AAO membranes with variable pore size grown in 2.7 wt% oxalic acid at 25-56V

V.II Immunocytochemistry

Figure 13 shows a micrograph of differentiated C17.2s on AAO membranes. All pore sizes were positive for β-tubulin III, nestin, and neurofilament H/M indicating a mixed phenotype population. β-tubulin III expression shows the presence of fully differentiated neurons, while nestin and neurofilament H/M mark cells that have not fully

differentiated. GFAP did not result in positive staining for any of the AAO membranes used in this experiment, indicating no astrocytic differentiation. The results indicate that the serum withdrawal process used to differentiate the cells did not result in full neuronal differentiation for the AAO membranes.

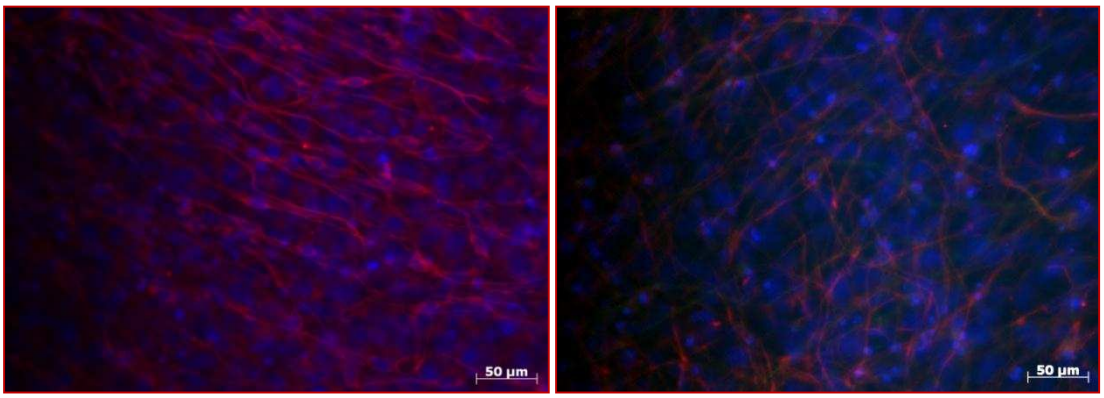

Figure 13. Differentiated C17.2 NSCs on AAO membranes stained for expression of nuclei (blue, circles) and neurofilament H/M (left) and nestin (right) shown in red

Figure 14 shows ICC images of C17.2s grown on AAO membranes and tissue culture treated (TCT) glass stained for β-tubulin III (green, extensions) and nuclei (blue, circles). TCT glass is a common cell culture substrate and was evaluated as a means to compare neuronal response of the AAO membranes to common methods. NeuronJ software was used to measure the neurite outgrowth lengths of the differentiated neurons on each of the substrates shown in Figure 14. Neurite outgrowth is commonly used as a measure of neuronal maturity and ability to communicate with other cells via synapses. Quantitative measurements of the neurite outgrowth lengths can be seen in Figure 15. Compared to the TCT glass control, all AAO membranes showed increased neurite outgrowth. The samples with the longest neurite outgrowth are the AAO membranes with pores in the 64-78nm range. The results suggest that there may be an optimum pore size

for promoting neurite outgrowth of C17.2s. The 78nm and 77nm pig-nosed membranes show similar neurite outgrowth behavior. This could potentially indicate that the inter-cell-wall distance is the dominant feature that the cells are responding to rather than the structure several nanometers into the pore opening where the inter-pore growth begins to be seen.

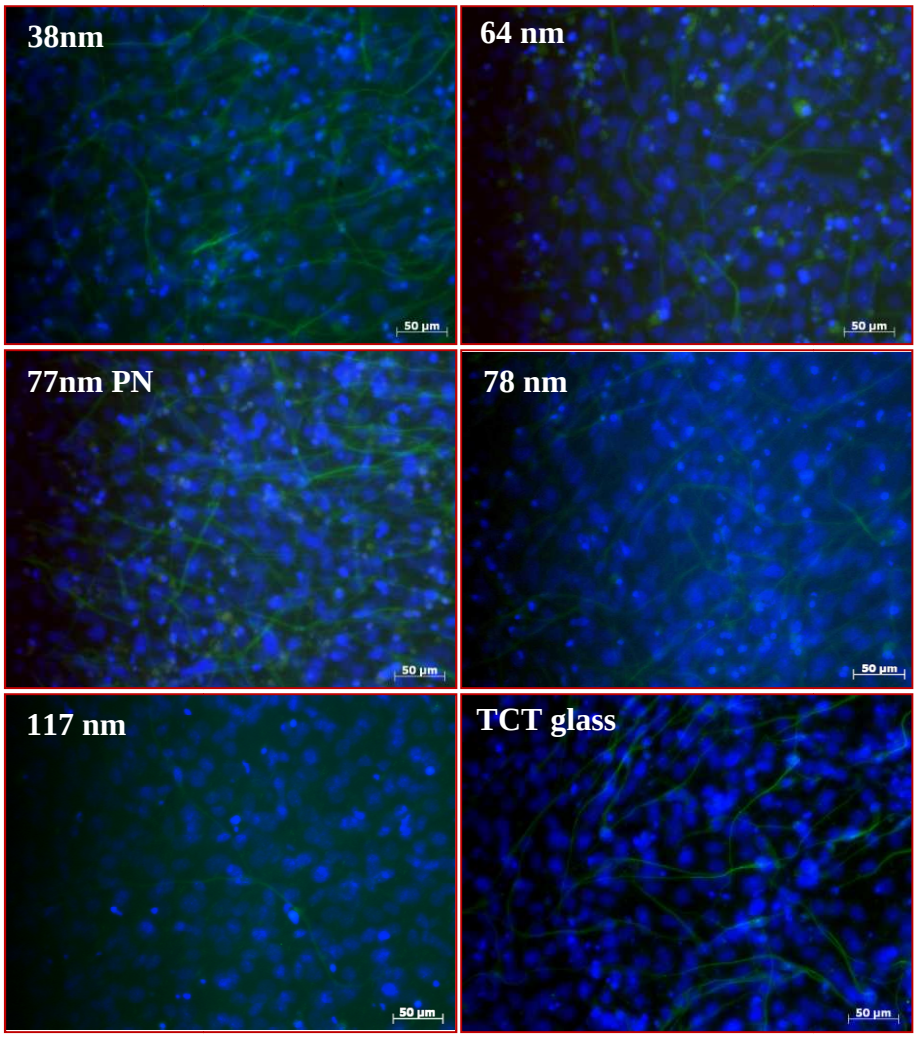

Figure 14. C17.2s differentiated on AAO membranes with various pore sizes as well as tissue culture treated glass and stained for β-tubulin III (green, extensions) and nuclei (blue, circles)

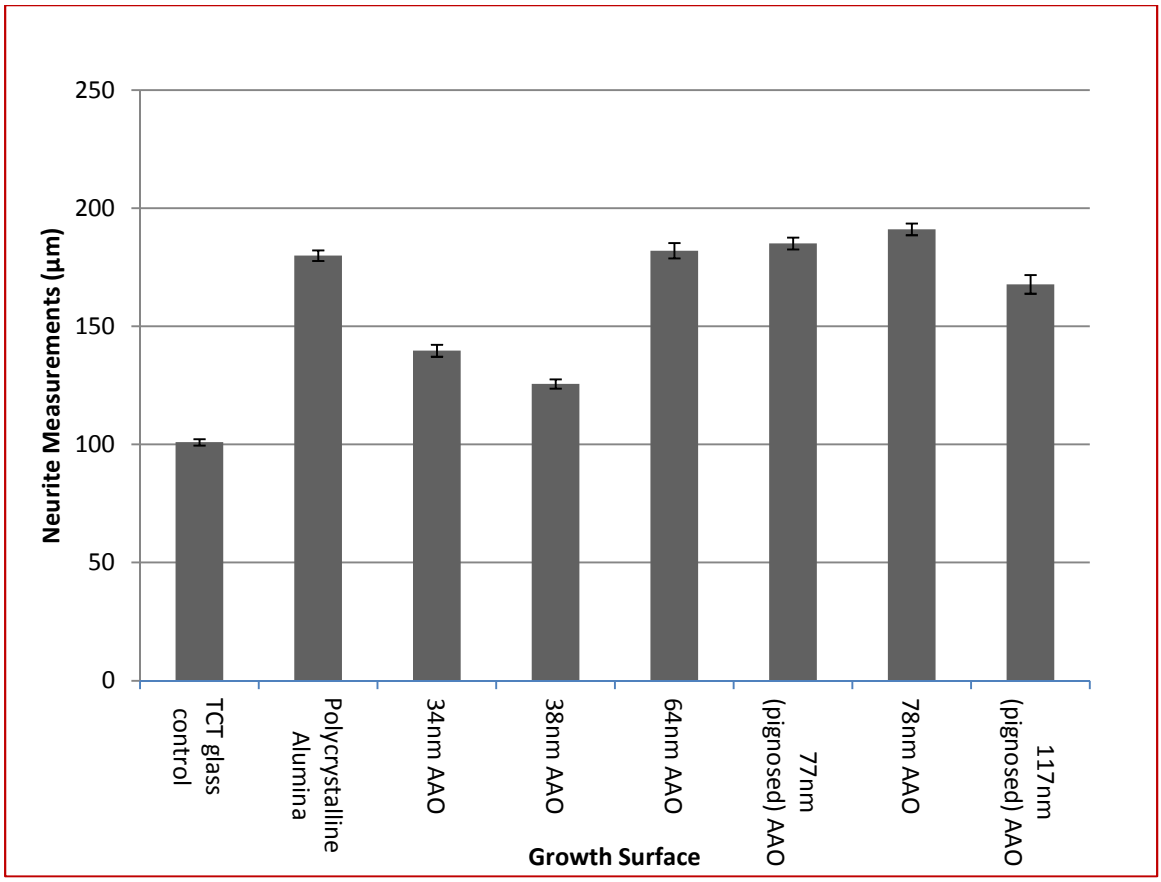

Figure 15. Neurite outgrowth measurements on each growth surface

Neurons differentiated on the polycrystalline alumina appears to have similar behavior to those grown on AAO with pore sizes between 64-78nm. Figure 16 shows an SEM image of the polycrystalline alumina surface prior to cell growth. The polycrystalline alumina surface has an irregular roughness. The surface exhibits features on a macro scale as well as sub-features on the nanometer scale. Additionally, the polycrystalline alumina has a similar chemistry to the AAO membranes. These properties resulted in similar neurite outgrowth to the AAO membranes.

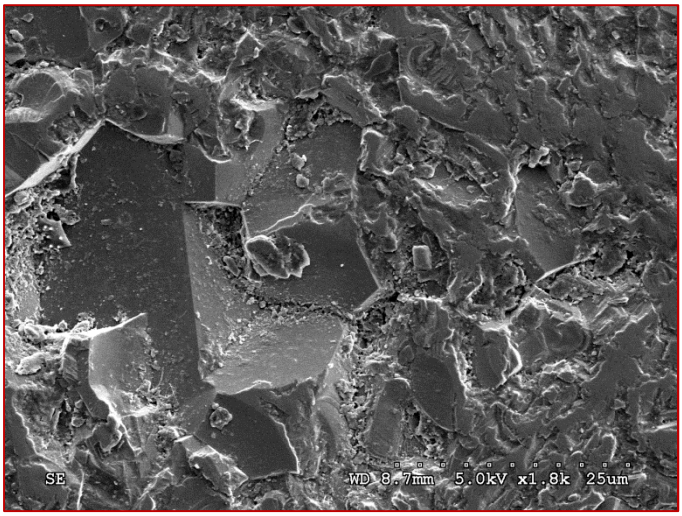

Figure 16. SEM micrograph of the polycrystalline alumina surface before cell growth

To gain some understanding of the mixed phenotype population present on the membranes neuronal populate percentages were calculated. Figure 17 shows the neuronal population percentages of C17.2s differentiated on AAO membranes and a TCT glass control. TCT glass showed the highest neuronal percentage, followed closely by the polycrystalline alumina and AAO membranes with 34nm and 38nm pores. In contrast, AAO membranes with larger pore sizes (above 64nm) showed significantly lower neuronal percentages. The results suggest a relationship between pore size and population dynamics. Additionally, the irregular surface roughness of the polycrystalline alumina seems to promotes neuronal differentiation more so than the AAO membranes.

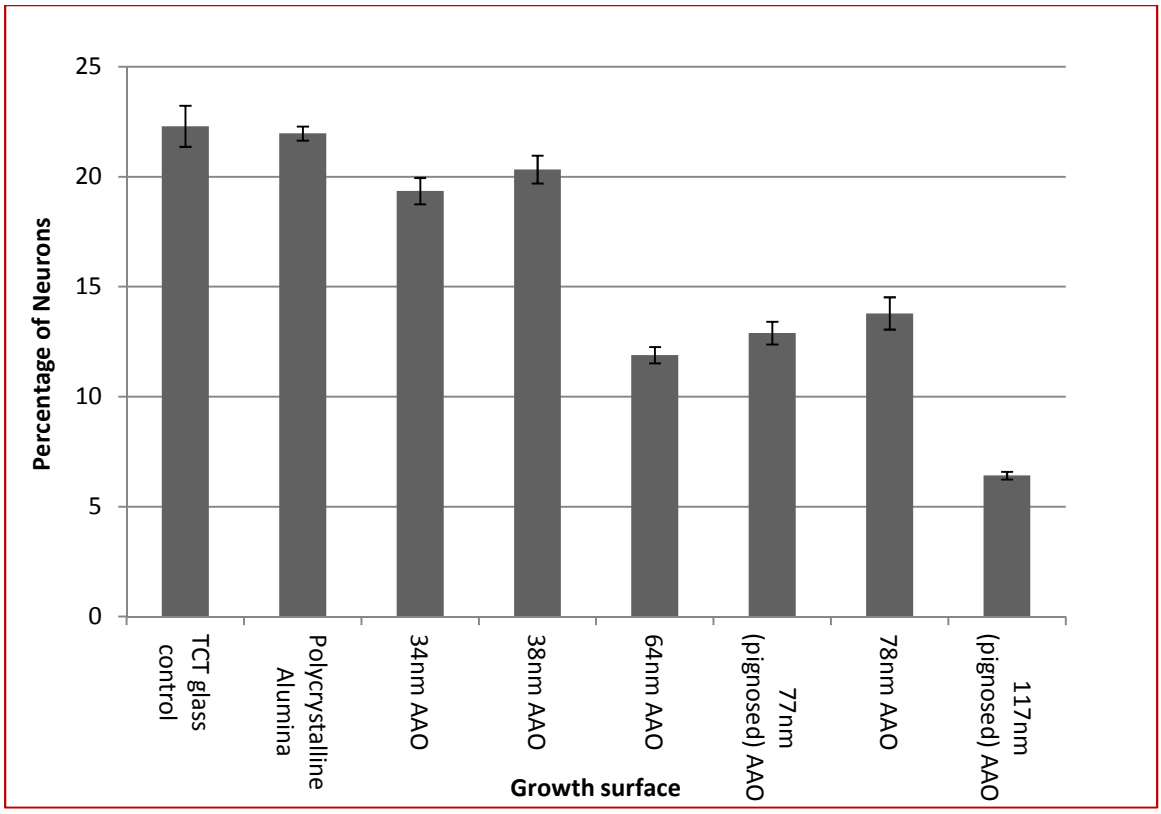

Figure 17. Neuronal population percentage of C17.2s differentiated via serum withdrawal on each growth surface

V.III SEM Analysis of Cell Culture

SEM was performed to examine the cell layer morphology and membrane features after cell culture. Figure 18 shows an AAO membrane with 64nm pores after soaking in cell culture media. The membrane was never seeded with cells in order to evaluate if the cell culture process altered or clogged the pore structure in any way. The membranes maintain their pore structure and experience no physical change in their dimensions/morphology from the cell culture process.

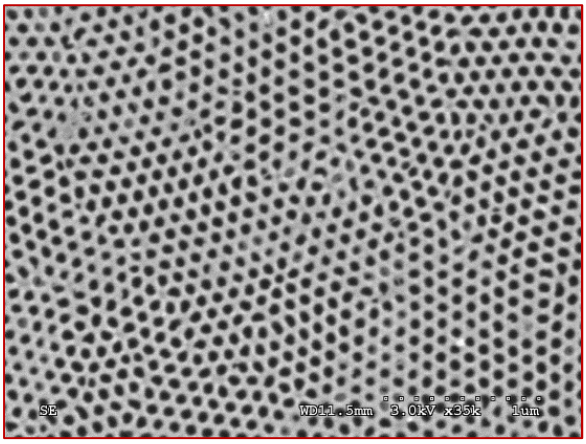

Figure 18. SEM micrograph of AAO membrane with 64nm pores examined after soaking in cell culture media

An SEM micrograph of the cell layer on TCT glass is shown in Figure 19. The cell layer is several microns thick, and interactions can be seen in between the neurons and the surface of the cell layer. Small focal adhesions were observed attaching the tissue layer to the TCT glass.

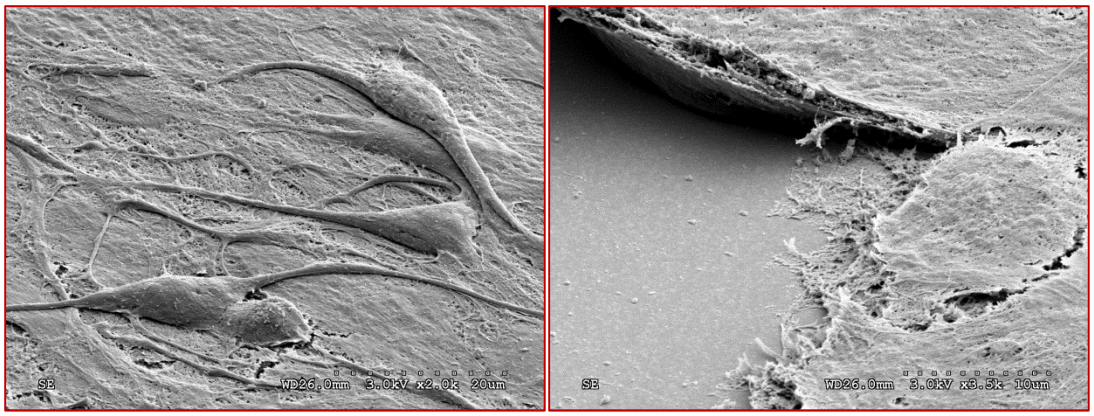

Figure 19. SEM micrographs of C17.2 cell layer after differentiation on TCT glass showing neuron interacting with the cell layer (left) and focal adhesions (right)

Figure 20 shows representative SEM micrographs of the cell layer found on AAO membranes after differentiation. The AAO membranes all showed similar cell layer morphology, regardless of pore size. A dense tissue-like layer was found that was thicker than that found on the TCT glass in most areas. Similar to the TCT glass, evidence was found of neuronal interaction with the cell layer. Morphological differences were also observed in the tissue layer on the AAO membranes supporting the mixed phenotype results from ICC.

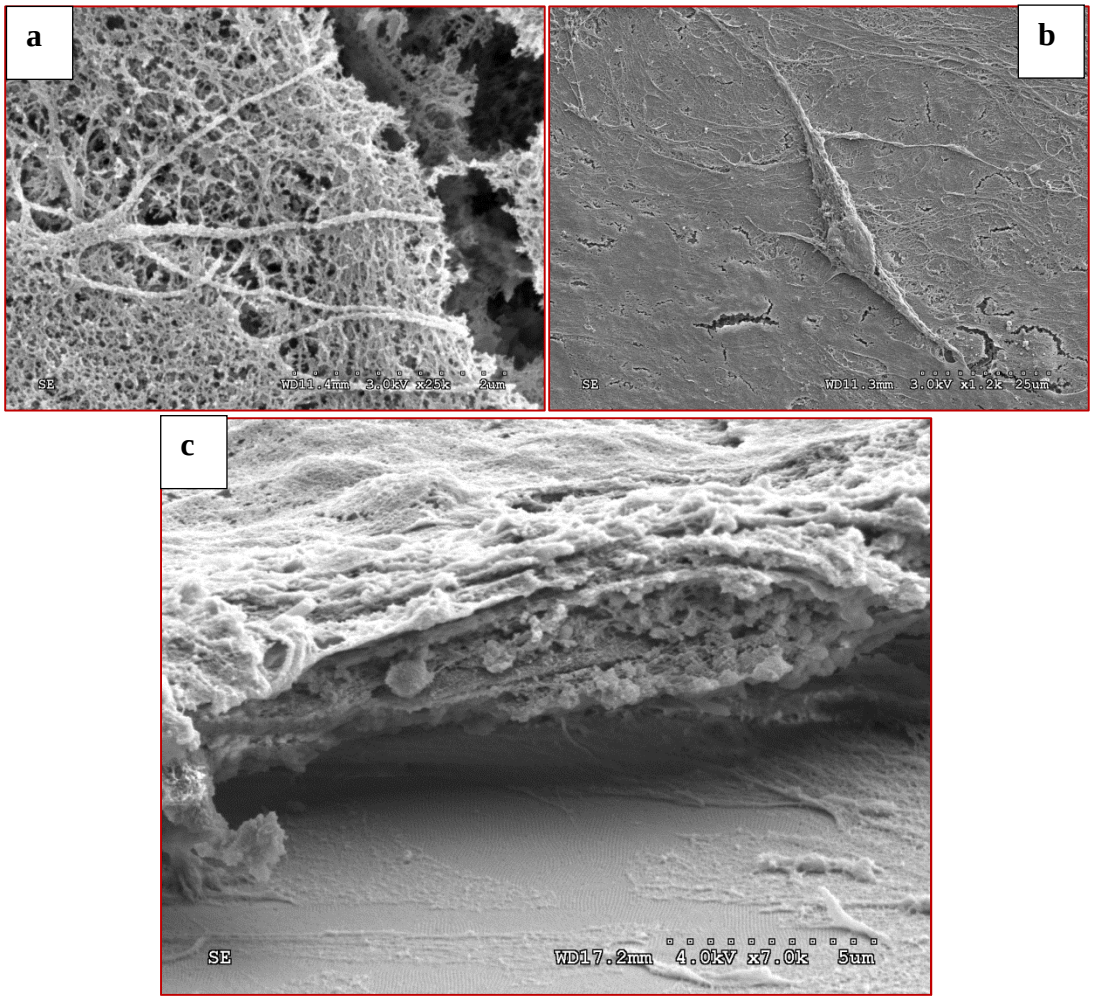

Figure 20. SEM micrographs of the cell layer on AAO membranes after differentiation showing a dense cellular growth (a) and neuronal interactions with the cell layer (b,c)

Figure 21 shows SEM micrographs of the cell interactions with the features on the AAO membranes. Neurons were found outstretched and interacting with the surface of the AAO membranes. Cells were seen to interact primarily with the surface of the membranes, and no evidence from SEM analysis suggests that the cells reach into the pore openings for the size range examined in this work. Figure 21c shows the edge of an AAO membrane after cell growth and suggests that the through-pore structure was in fact maintained throughout the cell culture process.

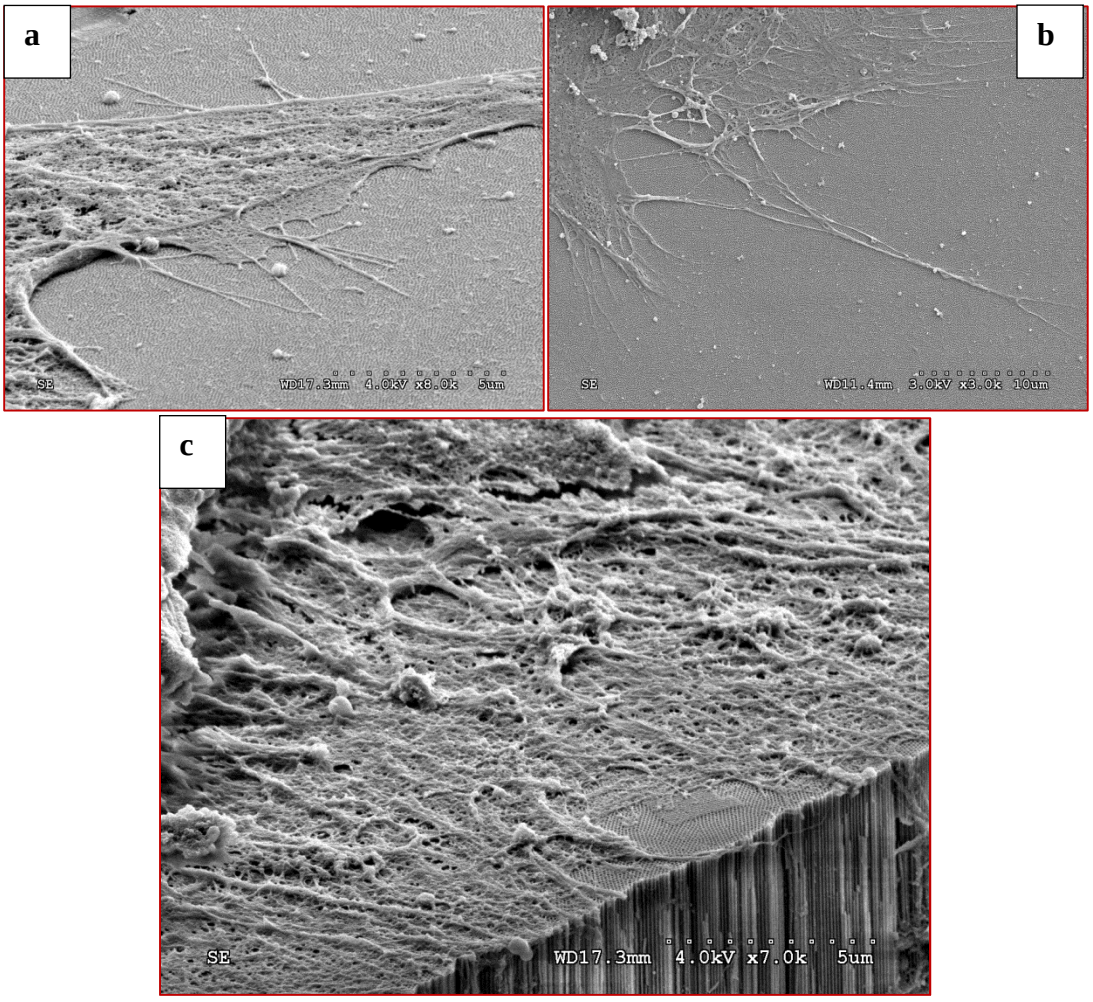

Figure 21. SEM micrographs of cell interactions with AAO membranes after differentiation (a,b) showing an intact through-pore morphology (c)

VI. Conclusions

AAO membranes were fabricated in 2.7% oxalic acid with varying pore diameters and seeded with C17.2 NSCs. AAO membranes with pore sizes ranging from 34-117nm were achieved. After cell culture and differentiation via serum withdrawal, the cellular response of the AAO was evaluated by ICC and SEM. The data suggests a highly tunable correlation between AAO pore diameter and differentiated cell populations. The following conclusions can be made based on the observed data:

1. AAO membranes support greater neurite outgrowth than TCT glass, regardless of pore size
2. Neuronal population varies with the pore size of AAO membranes, and the presence of a dense layer with mixed phenotypes suggests the possibility of tissue growth on AAO membranes
3. Through-pore morphology appears to be maintained indicating that AAO is a suitable candidate for an artificial cell/material synapse system

VII. Future Work

AAO membranes have been shown to have potential as highly tunable materials for cellular devices. It would be valuable to evaluate all steps in the AAO fabrication process for their influence on cellular response. The use of other electrolytes and other electrolyte concentrations opens up a much more significant range (10-300nm pore diameter) of ordered pores for study. The wide range of pores could allow for highly tunable surfaces which have very specific molecular selectivity in a cellular hybrid device. Surface modification techniques could also be incorporated once the basic

properties of AAO membranes from different fabrication methods are understood. As a precursor to understanding the complex variables in AAO fabrication, the next step of this study will be to perform XPS on the membranes fabricated for this experiment to fully understand the chemical configuration that the cells are interacting with.

The complex roughness of the polycrystalline alumina showed some interesting results as compared to the AAO membranes in this experiment. Future studies could incorporate patterned aluminum substrates to understand the effect of combinations of different surface features on AAO surfaces. It is possible that the benefits of promoting neurite outgrowth length could be combined with increased neuronal percentages to further tune the types of cells that differentiate on these engineered surfaces.

Finally, the results shown in this work showed great promise for tailoring cellular response of NSCs. It is likely, however, that different cell types will also have varied behavior on the AAO membranes. Expanding the types of cells studied on AAO membranes will widen the applications of AAO in biomedical devices. Additionally, from a scientific stand-point, understanding the response of other cell types on these materials could provide insight into the complex mechanisms by which AAO and it's morphology is affecting cell differentiation.

References

1. Kalpakjian, S. & Schmid, S. *Manufacturing Processes for Engineering Materials*. (Prentice Hall, 2007).
2. Thompson, G. . Porous anodic alumina: fabrication, characterization and applications. *Thin Solid Films* **297,** 192–201 (1997).
3. Keller, F., Hunter, M. S. & Robinson, D. L. Structural Features of Oxide Coatings on Aluminum. *J. Electrochem. Soc.* **100,** 411–419 (1953).
4. Hoar, T. P. & Mott, N. F. A mechanism for the formation of porous anodic oxide films on aluminium. *Journal of Physics and Chemistry of Solids* **9,** 97–99 (1959).
5. Diggle, J. W., Downie, T. C. & Goulding, C. W. Anodic oxide films on aluminum. *Chem. Rev.* **69,** 365–405 (1969).
6. O'Sullivan, J. P. & Wood, G. C. The Morphology and Mechanism of Formation of Porous Anodic Films on Aluminium. *Proc. R. Soc. Lond. A* **317,** 511–543 (1970).
7. Palibroda, E., Lupsan, A., Pruneanu, S. & Savos, M. Aluminium porous oxide growth. On the electric conductivity of the barrier layer. *Thin Solid Films* **256,** 101–105 (1995).
8. Patermarakis, G. & Tzouvelekis, D. Development of a strict kinetic model for the growth of porous anodic Al2O3 films on aluminum. *Electrochimica Acta* **39,** 2419–2429 (1994).
9. Parkhutik, V. P. & Shershulsky, V. I. Theoretical modelling of porous oxide growth on aluminium. *Journal of Physics D: Applied Physics* **25,** 1258–1263 (1992).
10. Shawaqfeh, A. T. & Baltus, R. E. Growth Kinetics and Morphology of Porous Anodic Alumina Films Formed Using Phosphoric Acid. *J. Electrochem. Soc.* **145,** 2699–2706 (1998).
11. Li, A. P., Müller, F., Birner, A., Nielsch, K. & Gösele, U. Hexagonal pore arrays with a 50–420 nm interpore distance formed by self-organization in anodic alumina. *Journal of Applied Physics* **84,** 6023–6026 (1998).
12. Belwalkar, A., Grasing, E., Van Geertruyden, W., Huang, Z. & Misiolek, W. Z. Effect of processing parameters on pore structure and thickness of anodic aluminum oxide (AAO) tubular membranes. *Journal of Membrane Science* **319,** 192–198 (2008).
13. Huang, Z., Zhang, W., Yu, J. & Gao, D. Nanoporous Alumina Membranes for Enhancing Hemodialysis. *Journal of Medical Devices* **1,** 79 (2007).
14. Crossland, A. C. *et al.* Residual flaws due to formation of oxygen bubbles in anodic alumina. *Corrosion Science* **41,** 1945–1954 (1999).
15. Masuda, H. & Fukuda, K. Ordered Metal Nanohole Arrays Made by a Two-Step Replication of Honeycomb Structures of Anodic Alumina. *Science* **268,** 1466–1468 (1995).
16. Masuda, H., Hasegwa, F. & Ono, S. Self□Ordering of Cell Arrangement of Anodic Porous Alumina Formed in Sulfuric Acid Solution. *J. Electrochem. Soc.* **144,** L127–L130 (1997).
17. Masuda, H. *et al.* Highly ordered nanochannel-array architecture in anodic alumina. *Applied Physics Letters* **71,** 2770–2772 (1997).

18. Nielsch, K., Choi, J., Schwirn, K., Wehrspohn, R. B. & Gösele, U. Self-ordering Regimes of Porous Alumina: The 10 Porosity Rule. *Nano Lett.* **2,** 677–680 (2002).
19. Choi, J. Fabrication of Monodomain Porous Alumina using Nanoimprint Lithography and its Applications. (2004).
20. Jessensky, O., Müller, F. & Gösele, U. Self-organized formation of hexagonal pore arrays in anodic alumina. *Applied Physics Letters* **72,** 1173–1175 (1998).
21. Bai, A., Hu, C.-C., Yang, Y.-F. & Lin, C.-C. Pore diameter control of anodic aluminum oxide with ordered array of nanopores. *Electrochimica Acta* **53,** 2258–2264 (2008).
22. Lee, W., Ji, R., Gösele, U. & Nielsch, K. Fast fabrication of long-range ordered porous alumina membranes by hard anodization. *Nat Mater* **5,** 741–747 (2006).
23. Le Coz, F., Arurault, L. & Datas, L. Chemical analysis of a single basic cell of porous anodic aluminium oxide templates. *Materials Characterization* **61,** 283–288 (2010).
24. Mardilovich, P. P., Govyadinov, A. N., Mukhurov, N. I., Rzhevskii, A. M. & Paterson, R. New and modified anodic alumina membranes Part I. Thermotreatment of anodic alumina membranes. *Journal of Membrane Science* **98,** 131–142 (1995).
25. Sui, Y. C., Cui, B. Z., Martínez, L., Perez, R. & Sellmyer, D. J. Pore structure, barrier layer topography and matrix alumina structure of porous anodic alumina film. *Thin Solid Films* **406,** 64–69 (2002).
26. Mardilovich, P. P., Govyadinoy, A. N., Mazurenko, N. I. & Paterson, R. New and modified anodic alumina membranes part II. Comparison of solubility of amorphous (normal) and polycrystalline anodic alumina membranes. *Journal of Membrane Science* **98,** 143–155 (1995).
27. McQuaig, M. K., Toro, A., Geertruyden, W. V. & Misiolek, W. Z. The effect of high temperature heat treatment on the structure and properties of anodic aluminum oxide. *J Mater Sci* **46,** 243–253 (2011).
28. Su, S.-H., Li, C.-S., Zhang, F.-B. & Yokoyama, M. Characterization of anodic aluminium oxide pores fabricated on aluminium templates. *Superlattices and Microstructures* **44,** 514–519 (2008).
29. Sulka, G. D., Stroobants, S., Moshchalkov, V., Borghs, G. & Celis, J.-P. Synthesis of Well-Ordered Nanopores by Anodizing Aluminum Foils in Sulfuric Acid. *J. Electrochem. Soc.* **149,** D97–D103 (2002).
30. Benedyk, J. Anodized Aluminum Oxide Applications as Nanomembranes and Nanotemplates in Electronic Devices, Energy Conversion, Sensors and Medicine. *Light Metal Age* **69,** 12–20 (2011).
31. De la Escosura-Muñiz, A. & Merkoçi, A. Nanochannels Preparation and Application in Biosensing. *ACS Nano* **6,** 7556–7583 (2012).
32. Losic, D. & Simovic, S. Self-ordered nanopore and nanotube platforms for drug delivery applications. *Expert Opinion on Drug Delivery* **6,** 1363–1381 (2009).
33. Du, Y. *et al.* Preparation and photoluminescence of alumina membranes with ordered pore arrays. *Applied Physics Letters* **74,** 2951–2953 (1999).
34. Eftekhari, A. *Nanostructured Materials in Electrochemistry*. (Wiley, 2008).

35. Mutalib Md Jani, A., Kempson, I. M., Losic, D. & Voelcker, N. H. Dressing in layers: layering surface functionalities in nanoporous aluminum oxide membranes. *Angew. Chem. Int. Ed. Engl.* **49,** 7933–7937 (2010).
36. Velleman, L., Triani, G., Evans, P. J., Shapter, J. G. & Losic, D. Structural and chemical modification of porous alumina membranes. *Microporous and Mesoporous Materials* **126,** 87–94 (2009).
37. Losic, D., Cole, M. A., Dollmann, B., Vasilev, K. & Griesser, H. J. Surface modification of nanoporous alumina membranes by plasma polymerization. *Nanotechnology* **19,** 245704 (2008).
38. Martin, C. R. & Kohli, P. The emerging field of nanotube biotechnology. *Nat Rev Drug Discov* **2,** 29–37 (2003).
39. Stojadinovic, S. *et al.* The effect of annealing on the photoluminescent and optical properties of porous anodic alumina films formed in sulfamic acid. *Applied Surface Science* **256,** 763–767 (2009).
40. Hiep, H. M., Yoshikawa, H. & Tamiya, E. Interference Localized Surface Plasmon Resonance Nanosensor Tailored for the Detection of Specific Biomolecular Interactions. *Anal. Chem.* **82,** 1221–1227 (2010).
41. Koutsioubas, A. G., Spiliopoulos, N., Anastassopoulos, D., Vradis, A. A. & Priftis, G. D. Nanoporous alumina enhanced surface plasmon resonance sensors. *Journal of Applied Physics* **103,** 094521–094521–6 (2008).
42. Alvarez, S. D., Li, C.-P., Chiang, C. E., Schuller, I. K. & Sailor, M. J. A Label-Free Porous Alumina Interferometric Immunosensor. *ACS Nano* **3,** 3301–3307 (2009).
43. Santos, A., Kumeria, T. & Losic, D. Nanoporous anodic aluminum oxide for chemical sensing and biosensors. *TrAC Trends in Analytical Chemistry* **44,** 25–38 (2013).
44. Pan, S. & Rothberg, L. J. Interferometric Sensing of Biomolecular Binding Using Nanoporous Aluminum Oxide Templates. *Nano Lett.* **3,** 811–814 (2003).
45. Takmakov, P., Vlassiouk, I. & Smirnov, S. Hydrothermally shrunk alumina nanopores and their application to DNA sensing. *Analyst* **131,** 1248–1253 (2006).
46. Tan, F. *et al.* A PDMS microfluidic impedance immunosensor for E. coli O157:H7 and Staphylococcus aureus detection via antibody-immobilized nanoporous membrane. *Sensors and Actuators B: Chemical* **159,** 328–335 (2011).
47. Cheng, M. S. *et al.* Development of an electrochemical membrane-based nanobiosensor for ultrasensitive detection of dengue virus. *Analytica Chimica Acta* **725,** 74–80 (2012).
48. Nguyen, B. T. T. *et al.* Membrane-Based Electrochemical Nanobiosensor for the Detection of Virus. *Anal. Chem.* **81,** 7226–7234 (2009).
49. Rai, V. *et al.* Ultrasensitive cDNA Detection of Dengue Virus RNA Using Electrochemical Nanoporous Membrane-Based Biosensor. *PLoS ONE* **7,** e42346 (2012).
50. De la Escosura-Muñiz, A., Chunglok, W., Surareungchai, W. & Merkoçi, A. Nanochannels for diagnostic of thrombin-related diseases in human blood. *Biosensors and Bioelectronics* **40,** 24–31 (2013).
51. Karlsson, M., Pålsgård, E., Wilshaw, P. . & Di Silvio, L. Initial in vitro interaction of osteoblasts with nano-porous alumina. *Biomaterials* **24,** 3039–3046 (2003).

52. Hu, J. *et al.* Cell culture on AAO nanoporous substrates with and without geometry constrains. *Microelectronic Engineering* **88,** 1714–1717 (2011).
53. Patermarakis, G. & Masavetas, K. Aluminium anodising in oxalate and sulphate solutions. Comparison of chronopotentiometric and overall kinetic response of growth mechanism of porous anodic films. *Journal of Electroanalytical Chemistry* **588,** 179–189 (2006).
54. Casey, M. E., Ventura, A. P., Misiolek, W. Z. & Jedlicka, S. Anodic Aluminum Oxide (AAO) Membranes for Neurite Outgrowth. *MRS Online Proceedings Library* **1498,** null–null (2013).
55. Snyder, E. Y. *et al.* Multipotent neural cell lines can engraft and participate in development of mouse cerebellum. *Cell* **68,** 33–51 (1992).
56. Snyder, E. Y., Taylor, R. M. & Wolfe, J. H. Neural progenitor cell engraftment corrects lysosomal storage throughout the MRS VII mouse brain. *Nature* **374,** 367–370 (1995).
57. Snyder, E. Y., Yoon, C., Flax, J. D. & Macklis, J. D. Multipotent neural precursors can differentiate toward replacement of neurons undergoing targeted apoptotic degeneration in adult mouse neocortex. *PNAS* **94,** 11663–11668 (1997).

Vita

Anthony Patrick Ventura was born in Columbia, Maryland on September 29, 1989. He is the son of Chris and Dale Ventura, and the younger brother of Dominic Ventura. In 2011, he graduated with high honors from Lehigh University with a Bachelor of Science in Materials Science and Engineering. Following his undergraduate studies, he stayed at Lehigh for graduate school where he earned his Master of Science in Materials Science and Engineering in 2013. After obtaining his M.S. degree, Anthony moved to Philadelphia, PA and continued working with Wojciech Misiolek at Lehigh University towards his Doctor of Philosophy in Materials Science and Engineering.

Contact: apv211@lehigh.edu